

Surface for methane combustion: $O(^3P)+CH_4 \rightarrow OH+CH_3$

Ya Peng(彭亚), Zhong-An Jiang(蒋仲安), Ju-Shi Chen(陈举师)

Citation: Chin. Phys. B . 2020, 29(7): 073401 . **doi:** 10.1088/1674-1056/ab90f5
Journal homepage: http://cpb.iphy.ac.cn; http://iopscience.iop.org/cpb

What follows is a list of articles you may be interested in

Collision of cold CaF molecules: Towards evaporative cooling

Yuefeng Gu(顾跃凤), Yunxia Huang(黄云霞), Chuanliang Li(李传亮), Xiaohua Yang(杨晓华)

Chin. Phys. B . 2019, 28(3): 033401 . **doi:** 10.1088/1674-1056/28/3/033401

Solvent effects and potential of mean force study of the S_N2 reaction of CH_3F+CN^- in water

Chen Li(李琛), Peng Liu(刘鹏), Yongfang Li(李永方), Dunyou Wang(王敦友)

Chin. Phys. B . 2018, 27(3): 033401 . **doi:** 10.1088/1674-1056/27/3/033401

Effects of collision energy and rotational quantum number on stereodynamics of the reactions: $H(^2S)+NH(v=0, j=0, 2, 5, 10)\rightarrow N(^4S)+H_2$

Wei Wang(王伟), Yong-Jiang Yu(于永江), Gang Zhao(赵刚), Chuan-Lu Yang(杨传路)

Chin. Phys. B . 2016, 25(8): 083402 . **doi:** 10.1088/1674-1056/25/8/083402

Stereodynamics of the reactions: $F+H_2/HD/HT \rightarrow FH+H/D/T$

Chi Xiao-Lin, Zhao Jin-Feng, Zhang Yong-Jia, Ma Feng-Cai, Li Yong-Qing

Chin. Phys. B . 2015, 24(5): 053401 . **doi:** 10.1088/1674-1056/24/5/053401

Theoretical study of stereodynamics for the $N+H_2/D_2/T_2$ reactions

Li Yong-Qing, Zhao Jin-Feng, Zhang Yong-Jia, Chi Xiao-Lin, Ding Yong, Ma Feng-Cai

Chin. Phys. B . 2014, 23(12): 123401 . **doi:** 10.1088/1674-1056/23/12/123401

Surface for methane combustion: $O(^3P) + CH_4 \rightarrow OH + CH_3$*

Ya Peng(彭亚)†, Zhong-An Jiang(蒋仲安)‡, and Ju-Shi Chen(陈举师)

School of Civil and Resource Engineering, University of Science and Technology Beijing, Beijing 100083, *China*

(Received 29 February 2020; revised manuscript received 28 April 2020; accepted manuscript online 7 May 2020)

Kinetic investigations including quasi-classical trajectory and canonical unified statistical theory method calculations are carried out on a potential energy surface for the hydrogen-abstraction reaction from methane by atom $O(^3P)$. The surface is constructed using a modified Shepard interpolation method. The *ab initio* calculations are performed at the CCSD(T) level. Taking account of the contribution of inner core electrons to electronic correlation interaction in *ab initio* electronic structure calculations, modified optimized aug-cc-pCVQZ basis sets are applied to the all-electrons calculations. On this potential energy surface, the triplet oxygen atom attacks methane in a near-collinear H–CH_3 direction to form a saddle point with barrier height of 13.55 kcal/mol, which plays a key role in the kinetics of the title reaction. For the temperature range of 298–2500 K, our calculated thermal rate constants for the $O(^3P) + CH_4 \rightarrow OH + CH_3$ reaction show good agreement with relevant experimental data. This work provides detailed mechanism of this gas-phase reaction and a theoretical guidance for methane combustion.

Keywords: methane combustion, potential energy surface, transition state, kinetic, *ab initio* electronic structure calculation

PACS: 34.10.+x, 31.15.xv, 34.50.Lf **DOI:** 10.1088/1674-1056/ab90f5

1. Introduction

Hydrocarbon combustion involves many kinds of chemical reactions, in which reactions of $O(^3P)$ with hydrocarbons play an important role in the key initial steps.[1–10] The reaction $O(^3P) + CH_4 \rightarrow OH + CH_3$ has been investigated in a lot of experimental and theoretical studies over the decades as a prototype of the hydrocarbon combustion.[11–18] In 2005, all of the available and recommended data was summarized.[19] The thermal rate constants was recommended as $k(T) = 7.3 \times 10^{-19} T^{2.3} \exp(-3310/T)$ $cm^3 \cdot molecule^{-1} \cdot s^{-1}$ over the temperature range from 400 K to 2500 K, while the measured rate constants were distributed widely below 400 K. It has also been investigated theoretically by using multifarious approaches.[11,20–23] The Jahn–Teller conical intersection has advanced nature and potential effectiveness.[1,20–22,24–26] Its appearance as the oxygen atom gets close to the hydrogen atom along the H–CH_3 bond has not only aroused great theoretical concern but also brought some uncertainty to kinetics. The 3-fold symmetry leads to a ^3E state, which could be split into one $^3A'$ and one $^3A''$ after the break of C_{3v} symmetry surface.[27–29] Recently our group reported a series of studies to obtain a better understanding of the reaction mechanisms and clarify the role of saddle point. The barrier heights of $^3A'$ and $^3A''$ first-order saddle points formed by $O(^3P)$ attacking hydrogen in the near-collinear H–CH_3 direction are 14.17 and 14.13 kcal/mol, respectively.[4–6] Our calculated imaginary frequency for the TS is 2376i in cm^{-1}, corresponding to a narrow potential barrier.

To achieve accurate kinetic investigation of the title reaction, an accurate potential energy surface (PES) is basically required.[25,26,30–32] A series of *ab initio* PESs for the title reaction have been constructed. Despite the first full dimensional analytical one (labeled as PES-1998) was constructed by Corchado and co-workers,[24] the most widely used one was constructed by Espinosa-Garcia and co-workers.[33] The PES-1998 was on the basis of studies by Joseph *et al.*[34] and Jordan *et al.*,[35] in which PESs were found to be not completely symmetric in all the potential energy terms pertaining to the four hydrogen atoms of CH_4. Later, the PES-2000 and PES-2014 for $O(^3P) + CH_4$ were reported,[25,33,36] especially the full-dimensional analytical PES-2014 by González–Lavado and co-authors which has been acted as a benchmark to test the accuracy of approximate theories[31,37–40] and can be applied to more complicated reactions. The PES-2014 predicts a barrier height of 14.0 kcal/mol with collinear O–H–CH_3 configuration. The ring polymer molecular dynamics (RPMD) method[41] and transition state theory with the least-action tunneling approximation (LAT) were employed to obtain the thermal rate coefficients of this reaction. The RPMD rate theory gives good estimate of quantum statistics in low temperature range and better one as the temperature goes higher.[26,41]

In this article, we present a ground-state PES for the $O(^3P) + CH_4 \rightarrow OH + CH_3$ reaction with the $^3A''$ transition state (TS) in gas phase. This PES is constructed with a modified Shepard interpolation scheme,[42,43] which has

*Project supported by the National Natural Science Foundation of China (Grant No. 51574016) and completed while the author was in residence at UNSW, Australia supported by the International Cooperation Training Program for Innovative Talents of USTB.

†Corresponding author. E-mail: pengyaustb@sina.com

‡Corresponding author. E-mail: jza1963@263.net

© 2020 Chinese Physical Society and IOP Publishing Ltd

been successfully applied in the PES construction of several polyatomic reactions, including $H+SiH_4$, $H+CH_4$ reaction systems.[44–48] Kinetic calculations obtained from this PES are compared in detail with previous available data. The methodology for the construction of PES are described in Section 2. The properties of the fitted surface are discussed and evaluated in Section 3. Section 4 discusses kinetic calculation results. Finally, a summary of the fitted PES is presented in Section 5.

2. Theoretical methodology

2.1. Electronic structure calculations

Extensive computational studies at different levels are performed in this work to investigate the PES of the $O(^3P)+CH_4 \rightarrow OH+CH_3$ reaction. The Gaussian 09 suite of *ab initio* programs[49] are chosen and used to perform all the *ab initio* calculations. The geometry coordinates, electronic structures symmetries and units for the reaction system defined in our previous work[4–6] are used throughout, unless otherwise specified. One of the major difficulties of the present work is to find a reasonable balance between *ab initio* accuracy and computational cost to yield smooth PESs and reaction barriers. A recent study by Truhlar *et al.* pointed out that the *ab initio* with all electrons taken into account and larger basis sets would give a fairly accurate description of the reaction barrier heights.[50] Good convergence could not be achieved when methods or basis sets are changed since the existence of PES crossing may make the estimate of saddle point unclear. This effect also appears in such a similar system as $O(^3P)+HF$ reaction, in which PES crossings originate from multiple states correlating to the triplet oxygen and intersect many times.[51] In fact, a completely satisfactory set for the global PES could neither be found by using higher level method nor by larger basis sets.

In our present work, the coupled-cluster singles and doubles approach plus quasi-perturbative triples excitations method, CCSD(T), is employed as it is suitable for accurate description of polyatomic molecules.[25,33,52] In order to reduce artificial error in the estimate of barrier height and long range region, the contribution of the inner core electron correlation effects for the energies are taken into account by using large and cost basis sets aug-cc-pCVQZ, which are modified and optimized in the form of (12s6p5d4f1g)/[7s6p5d4f1g][33,50] (the discussion of this *ab initio* scheme can be found elsewhere[4–6]). The paths of chemical reactions are followed by integrating the intrinsic reaction coordinate (IRC) with the Euler steepest-descent theory. The minimum energy path with a total of 196 calculated points is determined through IRC calculation from -1.9 a.u.$^{1/2}$Bohr on the reactant side to $+1.4$ a.u.$^{1/2}$Bohr on the product side, and it is shown schematically in Fig. 1 in which various stationary points are indicated.

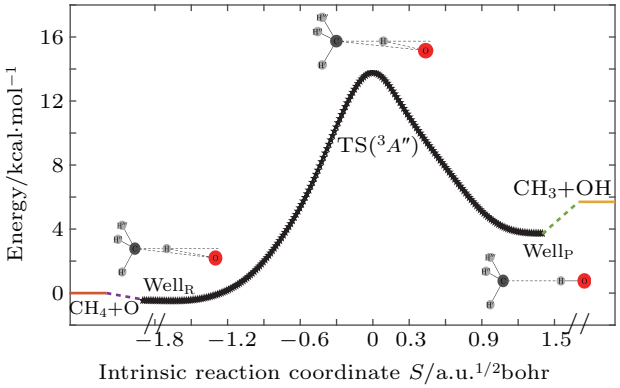


Fig. 1. $O(^3P)+CH_4(X^1A_1)$ reaction path obtained at the all-electron CCSD(T)/optACVQZ level. The energy of the reactants is set as zero.

2.2. Form of the PES

The energies, the energy first order derivatives and the energy second order derivatives at a set of data point geometries are employed to construct the surface with the modified Shepard interpolation method, which is proposed by Collins and has been successfully applied to many systems of more than four atoms for systematically generating *ab initio* PES.[42,43] A 2nd order Taylor series expansions is employed to represent the form of PES. The resulting continuous surface interpolates all the data points with all their corresponding symmetry equivalents in a $3N$-dimensional underlying surface landscape, which must be calculated at all data points scattered throughout the whole configuration space.

In the present work, the six-atom reaction system is represented using a general and straightforward system of coordinates given by linear combinations of inverse interatomic distances. It requires $0.5\times[6\times(6\text{-}1)]$ inverse interatomic distances Q_i to describe the positions of all atoms for the PES construction. Therefore, at a given configuration of the title reaction system and its all symmetry-equivalent copies, the optimal coordinates are defined as a vector $\boldsymbol{Q}=\{Q_1,Q_2,Q_3,\ldots,Q_{15}\}$. The final approximation to the surface is represented by the modified Shepard interpolation, which sums over all reference data and their symmetry equivalent configurations. The form of 2nd order local Taylor interpolation expansions $T_i(Q)$ centered on the set of N_{data} data point geometries is

$$\begin{aligned} T_i(Q) &= V[\boldsymbol{Q}(i)]+\sum_{k=1}^{3N-6}[\xi_k-\xi_k(i)]\frac{\partial V}{\partial \xi_k}|_{Q=Q_i} \\ &+\sum_{k=1}^{3N-6}\sum_{j=1}^{3N-6}0.5[\xi_k-\xi_k(i)] \\ &\times[\xi_j-\xi_j(i)]\frac{\partial^2 V}{\partial \xi_k \partial \xi_j}|_{Q=Q_i}, \end{aligned} \tag{1}$$

where

$$\xi_Q=\sum_{k=1}^{N(N-1)/2}U_{nk}Q_k \quad (n=1,2,3,\ldots,3N-6). \tag{2}$$

The final surface as a weighted average of these Taylor expansions is

$$V(Q) = \sum_{g \in G} \sum_{i=1}^{N_{\text{data}}} w_{goi}(Q) T_{goi}(Q), \tag{3}$$

where g is the group element; $g \in G$ means the inclusion of all elements g in a group G, which acts to interchange symmetry equivalent atoms; goi means that the ith configuration is transformed by g. Thus, the final and total symmetry of the reaction system is gained from their total direct product. The expressions for the normalized weight function $\omega_{goi}(Q)$ and $T_{goi}(Q)$, which weight the contribution of the Taylor expansion for each data point to the final surface energy function in the corresponding configuration space, have been discussed in detail elsewhere.[53,54]

2.3. Development of the surface

The selection of data points in Eq. (3) for the final Shepard interpolation is determined with the GROW2.2 package,[55] in which a set configurations are chosen as an initial start for generating subsequent coming points. This iterative method was developed by Collins and coworkers.[6,42,43,53] These points should provide an accurate picture that gives the accurate description of important chemical and kinetic regions in the reaction reactant side to the product side. Not only should the stationary points, points on minimum energy path and those close to the path be selected, but also more data points should be taken into account in view of physical considerations, particulary, the analysis of potential contour plots. For all these points, the electronic energies as well as the energy first and second order derivatives in all directions are obtained by *ab initio* calculations. From the initial points along the IRC, the size of data set will rise gradually by using the above iterative procedure. The iterative development in the construction of the surface is very efficient for polyatomic molecule reactions (the discussion of this iterative procedure can be found elsewhere[6,42,43,53]).

3. Properties of the PES

Our surface (denoted as PES-2019) is a 12-dimensional potential energy surface and constructed utilizing the methods illustrated above for hydrogen-abstraction reaction in the ground state from methane by triplet atom O. According to the quasi-classical trajectory (QCT) simulations proposed by Collins and Jordan,[42,43] the number of the data point sets chosen is several hundreds to thousands. The data set for the PES-2019 contains 9017 symmetry unique geometries. As the initial set, 196 geometries come from the IRC and 370 geometries are chosen carefully to accurately represent the region of interest, especially the important areas near the stationary points and van der Waals (vdW) areas. All the other geometries are determined by the QCT calculations. The central differences are employed to evaluate numerical Hessians to produce second derivative of energies at every small step. The QCT simulations concentrate on the geometries with the ∠OHC angle larger than 100° and the geometries near the region of reactant and saddle point (SP). To produce a sample of geometries for describing kinetic relevant region, more than two thousand of molecular configurations are picked up by randomizing the selection in the integration of trajectories generated from the reactant side. The average absolute error and the root-mean-square error (RMSE) from our surface are obtained to be 0.511 and 0.804 kcal/mol, respectively, which are quite smaller compared to the barrier height.

3.1. Weakly bound Interaction

This surface gives an accurate and clear topology of the regions close to the stationary points and the weakly bound interactions. The geometry parameters of various stationary points obtained from *ab initio* geometry optimizations and from the PES-2019 are collected in Tables 1 and 2, in which the available computational and experimental data from literature are also collected, while Fig. 2 shows the optimized geometries of the saddle point and vdW wells.

Table 1. Properties of reactants, products and saddle points on the PES-2019 for $O(^3P) + CH_4(X^1A_1) \rightarrow OH(X^2\Pi) + CH_3(X^2A_2'')$ in comparison with the previous reported data (all bond length in Bohr, bond angle and dihedral angle in degree, frequency in wave number and energy in kcal/mol).

	SP($^3A''$)				Reactants				Products			
	PES-2019 (a)	*ab initio* (b)	other (c)	other (d)	PES-2019 (a)	*ab initio* (b)	other (d)	Exp. (e)	PES-2019 (a)	*ab initio* (b)	other (d)	Exp. (e)
$V_{MEP}^{(f)}$	13.55	13.55	14.1	16.7(14.0)	0.0	0.0	0.0	0.0	5.49	5.49	5.70	
R_{OH}	2.216	2.214	2.268	2.253	30.0	30.0	–	–	1.832	1.832	1.835	1.8324
R_{CH}	2.643	2.643	2.417	2.470	2.104	2.102	2.058	2.062	30.0	30.0	–	–
$R_{CH'}$	2.097	2.090	2.073	2.050	2.104	2.102	2.058	2.062	2.033	2.033	2.039	2.039
$R_{CH''}$	2.097	2.090	2.073	2.050	2.104	2.102	2.058	2.062	2.033	2.033	2.039	2.039
$R_{CH'''}$	2.097	2.090	2.073	2.050	2.104	2.102	2.058	2.062	2.033	2.033	2.039	2.039
∠CHO	179.2	179.1	180.0	180.0	180.0	180.0	–	–	180.0	180.0	–	–
∠OCH′	103.3	103.8	–	–	109.5	109.5	109.5	109.5	90.0	90.0	–	–
∠OCH″	103.3	103.8	–	–	109.4	109.5	109.5	109.5	90.0	90.0	–	–
∠OCH‴	104.5	104.7	–	–	109.4	109.5	109.5	109.5	90.0	90.0	–	–
$\phi_{OHCH'}$	180.0	180.0	180.0	180.0	120.0	120.0	120.0	120.0	120.0	120.0	–	–
$\phi_{H'CHH''}$	120.2	120.2	–	–	119.8	119.9	120.0	120.0	120.0	120.0	–	–
$\phi_{H''CHH'''}$	122.3	122.6	–	–	119.8	119.9	120.0	120.0	120.0	120.0	–	–
$\phi_{H'''CHH'}$	120.3	120.6	–	–	120.1	120.1	120.0	120.0	120.0	120.0	–	–

Table 1. (*Continued*).

	SP($^3A''$)				Reactants				Products			
	PES-2019	*ab initio*	other	other	PES-2019	*ab initio*	other	Exp.	PES-2019	*ab initio*	other	Exp.
	(a)	(b)	(c)	(d)	(a)	(b)	(d)	(e)	(a)	(b)	(d)	(e)
$V_{MEP}^{(f)}$	13.55	13.55	14.1	16.7(14.0)	0.0	0.0	0.0	0.0	5.49	5.49	5.70	
υ_i	2315i	2315i	1919i	1900i	–	–	–	–	–	–	–	–
υ_1	228	228	417	404	1336	1336	1344	1306	597	598	491	606
υ_2	372	373	417	475	1336	1336			1396	1395	1430	1402
υ_3	519	520	591	582	1336	1336			550	1393		
υ_4	1049	1049	1000	1044	1561	1562	1570	1534	3022	3023	3126	3004
υ_5	1061	1061	1000	1163	1561	1562			3209	3209	3216	3171
υ_6	1159	1161	1044	1210	2941	2941	3035	2917	3205	3207	3289	
υ_7	1359	1357	1362	1496	3071	3077	3153	3019	3206	3204		
υ_8	1422	1422	1362	1518	3071	3077			3744	3739	3743	3738
υ_9	2992	2993	3019	3157	3071	3077						
υ_{10}	3119	3117	3168	3214								
υ_{11}	3136	3139	3168	3288								

(a) Reactants and products on the PES are optimized using the quasi-Newton method while the saddle point is located using the Newton-Raphson method; the frequencies are obtained by the normal-mode analysis;
(b) all-electron CCSD(T)/optACVQZ method;
(c) PES-2014 from Ref. [33];
(d) CCSD(T)=FC/cc-pVTZ values from Ref. [33] while values in parentheses at the CCSD(T) = FULL/aug-cc-pVQZ level;
(e) NIST Database from http://webbook.nist.gov/chemistry/;
(f) the energy of the reactants is set as zero.

Table 2. Properties of complexes at reactant side ($Well_R$, $Well'_R$) and product side ($Well_P$) and previous reported values (bond length in Bohr, bond angle and dihedral angle in degree, energy in kcal/mol and frequency in wave number).

	$Well_R$				$Well'_R$				$Well_P$			
	PES-2019	*ab initio*	other	other	PES-2019	*ab initio*	other	other	PES-2019	*ab initio*	other	other
	(a)	(b)	(c)	(d)	(a)	(b)	(c)	(d)	(a)	(b)	(c)	(d)
Energy$^{(e)}$	–0.53	–0.54	–0.5	–0.18	–0.59	–0.60	–0.3	–0.27	3.25	3.25	3.5	3.12
R_{OH}	6.012	6.012	5.629		9.074	9.077	6.315		1.858	1.843	1.842	
R_{CH}	2.103	2.106	2.056		2.102	2.105	2.050		4.835	4.838	4.318	
$R_{CH'}$	2.104	2.104	2.058		2.110	2.108			2.088	2.090	2.041	
$R_{CH''}$	2.104	2.104	2.058		2.110	2.108			2.088	2.090	2.041	
$R_{CH'''}$	2.104	2.104	2.058		2.110	2.108			2.088	2.090	2.041	
∠CHO	179.9	179.9	180.0		0.0	0.0	0.0		180.0	180.0	180.0	
∠OCH′	109.1	109.2			109.5	109.5			90.5	90.7		
∠OCH″	109.5	105.5			109.7	109.8			89.8	89.8		
∠OCH‴	109.5	105.5			109.7	109.8			89.8	89.8		
$\phi_{H'CHH''}$	120.1	120.1			120.1	120.1			120.0	120.0		
$\phi_{H''CHH'''}$	119.7	119.7			120.1	120.1			120.0	120.0		
$\phi_{H'''CHH'}$	120.1	120.1			120.1	120.1			120.0	120.0		
υ_1	57	57	42		50	50	65		57	57	85	
υ_2	78	78	72		86	85	98		130	130	123	
υ_3	78	78	99		113	113	100		160	160	156	
υ_4	1340	1340	1341		1399	1340	1401		301	301	293	
υ_5	1348	1348	1345		1467	1467	1410		335	335	323	
υ_6	1348	1348	1345		1467	1467	1410		593	593	570	
υ_7	1566	1566	1572		1787	1787	1777		1393	1393	1391	
υ_8	1566	1566	1572		1796	1796	1783		1399	1399	1418	
υ_9	3005	3005	3034		3133	3133	3134		3106	3107	3114	
υ_{10}	3016	3016	3152		3284	3284	3278		3224	3224	3285	
υ_{11}	3016	3016	3152		3331	3332	3327		3376	3375	3305	
υ_{12}	3019	3019	3159		3331	3332	3327		3610	3610	3650	

(a) Reactants and products on the PES are located using the quasi-Newton method; the frequencies are obtained by the normal-mode analysis;
(b) geometry optimization and vibrational frequency from all-electron CCSD(T)/optACVQZ method;
(c) CCSD(T) = FC/cc-pVTZ values from Ref. [33];
(d) benchmark from Ref. [25];
(e) the energy of the reactants is set as zero.

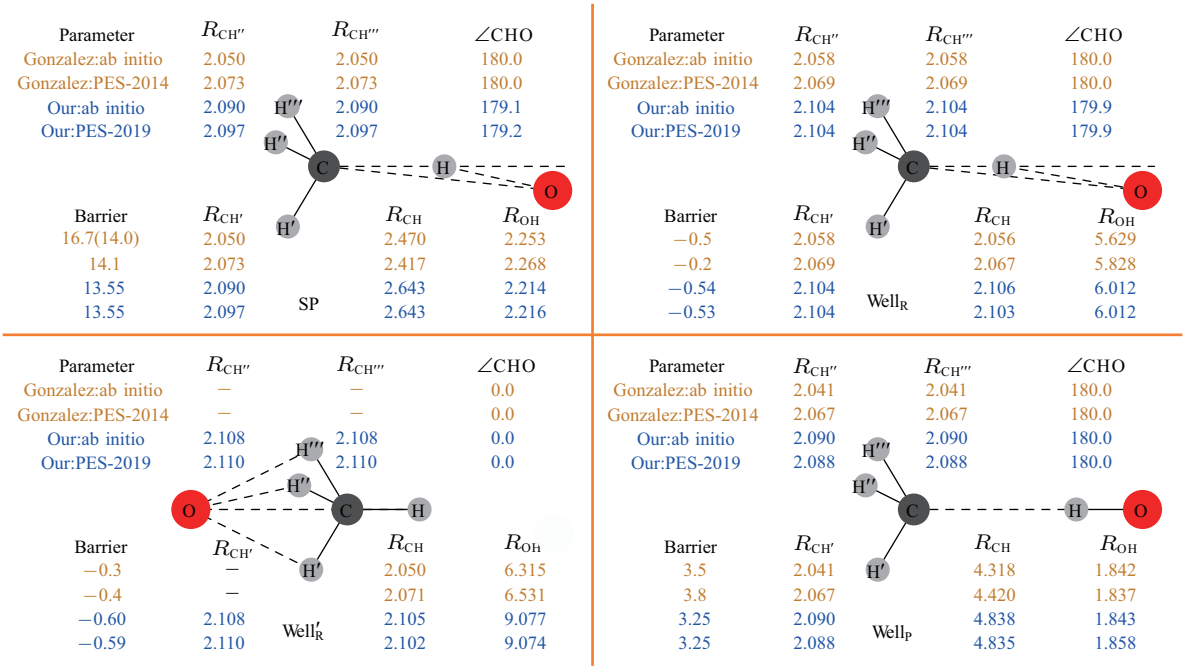


Fig. 2. Geometric parameters (distance in Bohr and angles in degree) of the saddle point (SP) and the intermediate complexes: $H_3CH\cdots O$ ($Well_R$), $O\cdots H_3CH$ ($Well'_R$) and $H_3C\cdots HO$ ($Well_P$).

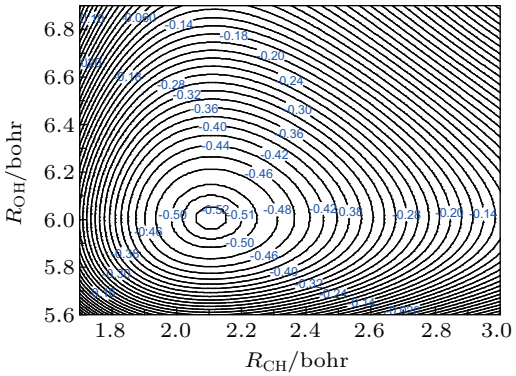


Fig. 3. Contour plot (kcal/mol) of the PES-2019 in the entrance channel. The energy of the reactants is set as zero.

The PES-2019 surface is a 12-dimensional hypersurface and not easy to be represented graphically. Several two-dimensional contour cut plots of the surface are made to check the reliability of our interpolation. Typical cuts of the PESs are shown in Figs. 3 and 4. The interaction of the O atom with methane leads to more than one vdW wells.[25,33,36] The van der Waals complexes play important roles in reaction dynamics.[56] The PES-2019 reproduces our previous *ab initio* calculations[4–6] in the long range interaction region to support a vdW potential well $H_3CH\cdots O$ ($Well_R$) in the entrance channel in Fig. 3, where the contour is plotted as a function of R_{OH} [1.6 Bohr, 3.0 Bohr] and R_{CH} [5.6 Bohr, 6.9 Bohr]. The present PES properly describes the structure of $Well_R$ since it has been identified to be reactive by the IRC calculation to connect to the corresponding saddle point. Moreover, several dozens of points around it have been chosen carefully in the initial set. The second vdW potential well $O\cdots H_3CH$ ($Well'_R$) is optimized and confirmed by frequency calculation but no IRC is found to connect with. Although additional (nearly one hundred) nearby points are taken into account in our PES construction, the contour plot of regions around the $Well'_R$ is still not as smooth as that of $Well_R$. The depth of reactant well $Well_R$ obtained from the PES-2019 is −0.53 kcal/mol, which corresponds to a vdW interaction between the triplet O atom and CH_4. It is weakly bounded but helpful to orient the reaction toward $Well_R$ as the $O\cdots H$–C axis.

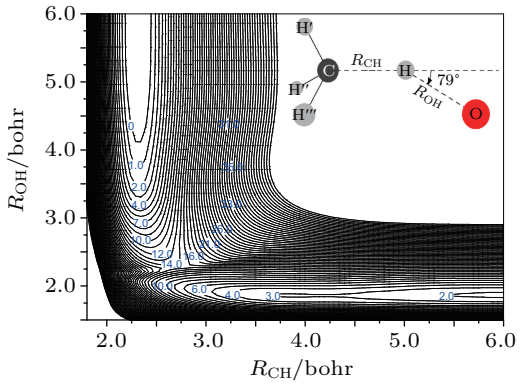


Fig. 4. Contour plot (kcal/mol) of the PES-2019 in the region around the transition state as functions of R_{CH} and R_{OH}. The energy of the reactants is set as zero.

3.2. Saddle point

A quasi-collinear $O\cdots H\cdots CH_3$ transition state appears when the triplet oxygen atom gets close to the one of four hydrogen atoms along a carbon hydrogen bond after the reactant well. The saddle point geometry in the title reaction has been somewhat uncertain for a long time.[57] Three saddle points for the $CH_4 + O(^3P) \rightarrow OH + CH_3$ reaction have been identified by more extensive electronic structure determinations in

our previous work,[4,5] and it plays a key role in the kinetics of the reaction. Under C_s symmetry, two SP^{1st} are identified in two symmetries $^3A''$ and $^3A'$, respectively. They get separated by one second-order $SP^{2nd}(^3E)$ that arises on account of the C_{3h} symmetry Jahn–Teller coupling. In the present work, the first two lowest saddle points are optimized and have a length of the breaking carbon hydrogen bonds of 2.643 and 2.649 Bohr, respectively. The barrier height of the lowest $SP^{1st}(^3A'')$ is 0.04 kcal/mol lower than that of the second lowest one $SP^{1st}(^3A')$. The lowest $SP^{1st}(^3A'')$ with the IRC through it and some points around it are taken into account in the initial set. In the surface construction, the second lowest $SP^{1st}(^3A')$ is also taken into account but without IRC or any other points around it. Since one $^3A''$ and one $^3A'$ surface propagate through the corresponding saddle point region, respectively, and correlate with the same ground-state products, it is assumed in the present work that the following rate constants are multiplied by 2 times with the consideration of the flux through the relative lower $^3A''$ surface. This approach has been employed in some previous reports.[22,36] All discussions in this paper refer to the $^3A''$ surface unless otherwise stated.

A comprehensive comparison of barrier heights from various reported references and our calculations is represented in Fig. 5. The barrier height obtained from our surface is 13.55 kcal/mol, which is close to the best estimated value 14.08 kcal/mol,[25] value 14.0 kcal/mol from the PES-2014[33] and our previous reported theoretical value 14.13 kcal/mol from CASSCF calculation.[4] The previous *ic*MRCI+*Q* *ab initio* calculations[4] give a barrier height (without zero-point-energy) much lower than the present CCSD(T) = FULL/optACVQZ, which may due to the following two reasons. First, the previous *ic*MRCI+*Q* value for the barrier height was obtained by single point energy calculation without full geometry optimization. Second, the CCSD(T) = FULL/aug-cc-pCV*X*Z (X = D, T, Q) calculations show a dramatic influence of basis set on the description of correction energies for the barrier height. It is clearly demonstrated that the barrier height has a downward tendency with further basis set extension.

In comparison with the high-accurate *ic*MRCI+*Q* calculations,[4] the CCSD(T) calculations in the present work give a lower saddle point, which overestimates the rate constant determined by the TST-based methods for the title reaction. On the other hand, the subtle aspects topology derived from the surface based on the CCSD(T) calculations gives a better description than those points (or curve) obtained from *ic*MRCI+*Q*. The rate constant calculations from our surface tend to average out the above two effects.

Contour plot (kcal/mol) for the PES-2019 in the region around the lower saddle point as functions of R_{CH} and R_{OH} is presented in Fig. 4. The length of the breaking carbon hydrogen bond of transition state on the PES-2019 is 2.643 Bohr, being 25.6% (0.539 Bohr) longer than that of the CH_4 molecule at equilibrium geometry as shown in Table 1. In Fig. 5 of Ref. [33], the energy of the PES-2014 rises much slowly but straightly as the system moves from the entrance/exit channel to the saddle point. In our Fig. 4, however, the energy is not slow or direct toward the saddle region. The different surface shapes of the transition state could be caused not only by differences of the barrier heights discussed above, but also by the differences of the imaginary frequencies. The imaginary frequencies at the transition states for the PES-1998, PES-2000, and PES-2014 are 1507i,[24] 1549i,[36] and 1919i[33] cm^{-1}, respectively. It is clear that the PES-2014 has the thinnest potential energy barrier among them. The harmonic frequencies calculated on the PES-2019 agree well with *ab initio* ones and give an imaginary frequency of 2315i cm^{-1}.

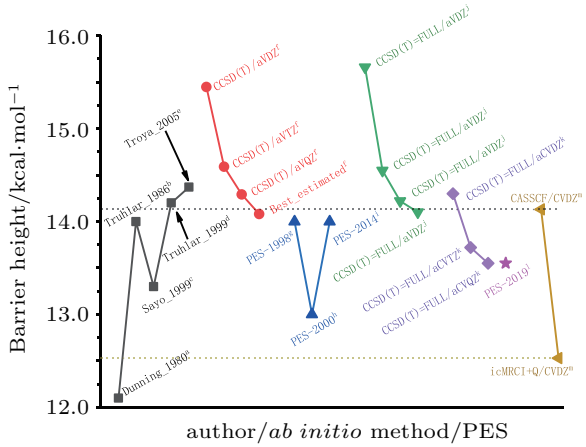


Fig. 5. The comparison of barrier heights from various reported references and our calculations. a: from Ref. [11]; b: from Ref. [61]; c: from Ref. [21]; d: from Ref. [22]; e: from Ref. [17]; f: from Ref. [25]; g: from Ref. [24]; h: from Ref. [36]; i: from Ref. [33]; j: present work at the CCSD(T) = FULL/ACV*x*Z (x = d, t, q, and 5) level; k: present work at the CCSD(T) = FULL/optACV*x*Z (x = d, t, and q) level; l: present work PES-2019; m: from Ref. [6].

Although some noticeable discrepancy can be observed in contour plots in Fig. 5 of Ref. [33] and Fig. 4, as well as in the description of the second vdW well O···H_3CH, both surfaces are broadly similar in the overall region. Besides slightly different aspect of *ab initio* calculation, the main difference between the PES-2014 and PES-2019 is also caused by different approaches used in surface constructions. The former is constructed using an analytical polynomial which is basically a valence bond-molecular mechanics, while the latter using interpolation method, which may not be suitable for weakly bound interactions but can be improved by adding more points on interested regions. The contour lines in Fig. 4 are smooth and without artificial oscillations in various regions. Although the smooth procedure has little effect on quantum kinetics, it can make a big difference on the QCT calculations.

4. Kinetic calculations

Some quasi-classical trajectory calculations have been performed on the prior version of this surface to study the vibrational distributions.[6] The prior version was constructed with 6100 symmetry unique geometries and it is converged. The main difference is that more points near potential wells were taken into account in the PES-2019 construction to give a better description of the weakly bound interactions. For the pair-correlated $CH_3(v=0)+OH(v'=0)$ products, the characteristics of angular distributions were analyzed by the QCT calculations. These results including the angular distributions of the $OH+CH_3$ products indicate that the distinct backward scattering are fully stronger than other directions. The angular distribution of the OH product represents a predominantly sharply backward scattering peak relative to the $O(^3P)$ beam direction, where no forward scattering peak or any signal from the sideways scattering is presented. This agrees well with the experimental measurement that about 90% of the total available energy remains as OH co-products rotations.[1,57] The QCT calculations on the PES-2019 in the present work and those[6] on its prior version are very similar and no observable divergence is found in the dynamic calculations, so similar dynamics results were excluded in the present manuscript to avoid redundancy. More dynamics properties have been calculated on the PES-2019 and compared with previous theoretical and experimental information.

4.1. Probability of reaction

To evaluate the reaction probability of $O(^3P)+CH_4\rightarrow OH+CH_3$, the QCT calculations are carried out on the PES-2019. For the following calculations, the initial CH_4 in its ground rovibrational state is used for all trajectories. The QCT calculations are started with the fragments separation of 30.0 Bohr for the reactants asymptote $O(^3P)+CH_4$. In the same way, the trajectories are stopped at products asymptote $OH+CH_3$ of 30.0 Bohr. The integration time step in the above calculation is set as 0.05 fs. Figure 6 shows the reaction probability (derived from one thousand trajectories) as a function of the N_{data}. The reaction probability does not provide much clue about the accuracy of the PES but gives some validation to check the convergence of PES. The reaction probability is multiplied by a factor of 4 during calculations since all the hydrogen atoms in methane contribute equally and are treated as distinguishable. Thus, the values of reaction probability in Fig. 6 already include a factor of 4. When the reference data set is grown to about 5000 points by the classical kinetic calculations, our obtained reaction probability does not go up and down eventually, and converges to 0.12 with very small changes. At 300 K, when E_{col} is set to be 30.0 kcal/mol for the title reaction, about 600000 trajectories are obtained with b_{max} of 5.0 Bohr. The maximum impact parameter b is the largest value of the impact parameter, which is determined by increasing its value until no new reactive trajectory is obtained. To test the reliability of these parameters for the QCT calculations, nearly a same number of trajectories are computed at several temperatures including 100 K, 200 K, and 500 K, and these results are very similar.

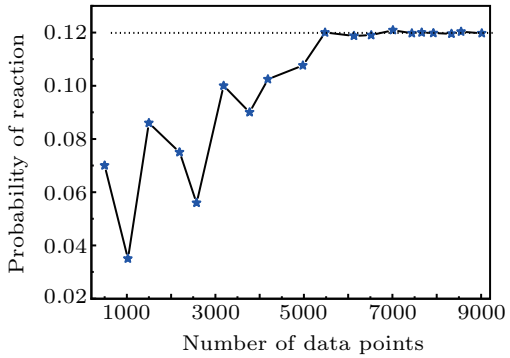


Fig. 6. The probability of reaction for $O(^3P)+CH_4(X^1A_1)\rightarrow OH(X^2\Pi)+CH_3(X^2A_2'')$ represented as a function of N_{data}. The dotted line displays the average value for $N_{data}=7012$, 7440, 7661, 7923, 8333, 8550 and 9017.

4.2. Thermal rate constant prediction

The traditional transition-state theory (denoted as TST) and canonical variational TS (denoted as CVT) theory calculations have been applied into this reaction, as well as canonical unified statistical (denoted as CUS) theory.[4,6] The spin–orbit (SO) coupling of the triplet oxygen atom and singlet methane molecular are integrated in the TST, CVT and CUS theory calculations using the POLYRATE 2015 program, which is a general polyatomic rate constants code and has been successfully employed to many polyatomic molecule reactions.[58] In the mass-weighted Cartesian coordinates, the reaction path starts from the highest point of transition state and goes gradually to the reactants side or in the opposite direction to products side. The effect of tunneling for rate constant calculations is taken into account by using the small-curvature tunneling (denoted as SCT), large-curvature tunneling (denoted as LCT) and LAT.

The thermal rate constants of hydrogen-abstraction reaction have been calculated at different temperatures ranging from 298 K to 2500 K, which are plotted in Fig. 7. It can be concluded from this figure that the thermal rate constants show typical Arrhenius behavior at temperatures of 298–2500 K for the $O(^3P)+CH_4\rightarrow OH+CH_3$ reaction. The newly obtained rate constants at 300 K, 600 K and 1000 K are 8.91×10^{-18} $cm^3\cdot molecule^{-1}\cdot s^{-1}$, 4.32×10^{-15} $cm^3\cdot molecule^{-1}\cdot s^{-1}$, and 1.22×10^{-13} $cm^3\cdot molecule^{-1}\cdot s^{-1}$, respectively, by using the basic canonical variational method. Compared with the previously reported values based on the PES-2014 (1.32×10^{-17} $cm^3\cdot molecule^{-1}\cdot s^{-1}$ with CUS/LAT or 1.50×10^{-17} $cm^3\cdot molecule^{-1}\cdot s^{-1}$ with RPMD) at 300 K,[59] our rate constant value agrees better with the experimental data from

the reported work[12,60] (5.50×10^{-18} cm^3·molecule^{-1}·s^{-1} -9.00×10^{-18} cm^3·molecule^{-1}·s^{-1}). This rate constant difference derived from the PES-2014 and PES-2019 is due to the different barrier heights as discussed in Section 3.2. The barrier height of our new surface is 0.05 kcal/mol lower than the benchmark value. As we know, the lower the barrier is, the larger the TST rate constants will be. The CVT and CUS are based on the TST method, but differ in the location of the transition state from TST. The other possible relative maxima and re-crossing are also taken into account in the CUS calculations, which reduce the rate constant values.

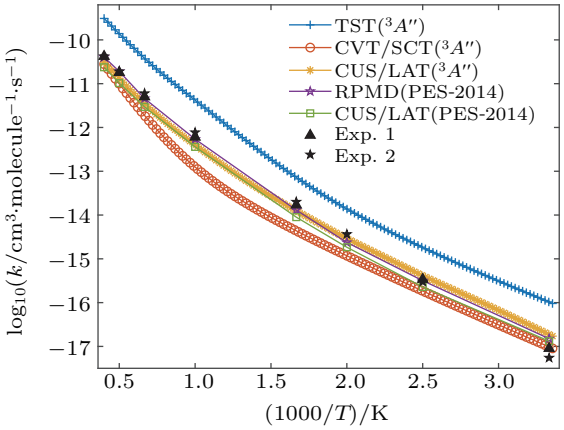


Fig. 7. Arrhenius plot for the CH$_4$+O(^{3}P) → CH$_3$+OH reaction. RPMD(PES-2014) and CUS/LAT(PES-2014): RPMD and CUS/LAT calculations with PES-2014 from Ref. [59]; Exp. 1: Experimental values from Ref. [60]; Exp. 2: Experimental values from Ref. [12].

The variational effects are induced into CVT calculations by optimizing the dividing surface to minimize the rate constant. The above reasons could account for that the TST rate constants are much larger than those of CVT and CUS.

Under 300 K, our CUS/LAT results are larger than the data of the previous corresponding work obtained on the PES-2014, while at high temperatures ours are smaller. The RPMD rate theory is believed to be exact in the classical high-temperature limit, *e.g.*, 2500 K, it gives the rate constant with the PES-2014 as 4.05×10^{-11} cm^3·molecule^{-1}·s^{-1}, which is very close to the experimental data 4.20×10^{-11} cm^3·molecule^{-1}·s^{-1}. The CUS/LAT calculations on the PES-2014 and PES-2019 give the value of 2.37×10^{-11} cm^3·molecule^{-1}·s^{-1} and 3.00×10^{-11} cm^3·molecule^{-1}·s^{-1}, respectively. Notwithstanding at low-temperature 300 K and high-temperature 2500 K the calculated rate constants obtained from the PES-2019 are better than those from the PES-2014 using the same method, we cannot deny that the rate constants of the PES-2019 and PES-2014 at the most temperature are pretty close contest. In particular, the rate constant difference between our CUS/LAT on the PES-2019 and RPMD (or CUS/LAT) on the PES-2014 becomes very small as the temperature goes higher, which shows that all quantum mechanical effects in practice become virtually invisible. On the whole, both the results are in basic agreement with the available experimental work.

The ratio of the rate coefficients of the unsubstituted reaction to the deuterated reaction, CH$_4$/CD$_4$, is obtained to analyze the kinetic isotope effects (KIEs) which depend on the masses of reactants. The KIEs at different temperatures obtained from various PESs are listed in Table 3. It has been pointed out that the KIE is less sensitive to the accuracy of the PES, but a very sensitive test of dynamics approaches.[59] As far as we know, not only are the experimentally determined isotope data not available for comparison but also the various theoretical reported values are wildly different. Our calculated KIEs from CVT/SCT and the previous works show similar trends, but their values do not agree well. Although, in general, the present KIEs values obtained from CUS(PES-2019) are lower than the RPMD/CUS calculation on the PES-2000/PES-2014,[59] all these KIEs decrease rapidly as the temperature goes higher in the whole temperature range. This phenomenon is explained by Zhao and co-workers.[31] The quantum tunneling effect of the H atom increases more rapidly than that of the heavier D atom, which makes the difference between the rates of O + CH$_4$ and O + CD$_4$ larger and larger with decreasing temperature.

Table 3. H/D kinetic isotope effects (KIEs) for the O(^{3}P) + CH$_4$/CD$_4$ reaction.

Method	Temperature/K			
	300	600	1000	2500
CUS/LAT(PES-2019)[a]	12.276	2.081	1.057	0.985
Quantum Instanton(PES-2014)[b]	45.60	5.25	2.24	–
RPMD(PES-2014)[c]	30.8	3.8	2.0	1.1
CUS/LAT(PES-2014)[c]	18.6	2.4	1.43	1.10
Quantum Instanton(PES-2000)[b]	18.04	3.88	2.23	–
CUS/μOMT(PES-2000)[d]	18.9	3.4	1.4	0.93
Quantum Instanton(PES-1998)[b]	16.64	3.38	2.16	–
CUS/μOMT(PES-1998)[e]	29.1	4.2	1.78	1.22

[a]Present work; [b]Ref. [31]; [c]Ref. [59]; [d]Ref. [36]; [e]Ref. [24];
TST: transition-state theory calculations;
CVT: canonical variational transition-state theory calculations;
CUS: canonical unified statistical theory calculations;
RPMD: polymer molecular dynamics approach calculations;
SCT: smallcurvature-tunneling;
LAT: least-action tunneling.

5. Summary

We have carried out kinetic studies of hydrogen-abstraction reaction of CH$_4$ + O(^{3}P) on a 12-dimensional PES. This PES is based on extensive all electrons CCSD(T) method of *ab initio* theory together with basis sets of modified optimized aug-cc-pCVQZ. The modified Shepard interpolation is used to construct the interpolated PES, of which the best RMSE is 0.804 kcal/mol and all the contour plots are smooth. The classical trajectories are calculated on this surface to check the PES convergence. The canonical variational and

statistical theory for thermal rate constant calculations are also carried out on the PES-2019, and it is encouraging to see better agreement between the computed CUS/LAT rate constants and the available experimental measurements. This PES shows that the triplet oxygen atom attacks methane in a near-collinear H–CH_3 direction to form a saddle point with barrier height of 13.55 kcal/mol. The property analysis in various regions shows the PES-2019 surface is physically reasonable.

The construction of PES with the $^3A''$ TS and the corresponding rate constants discussed in this work can contribute to a full understanding of the kinetics of reaction $O(^3P) + CH_4 \rightarrow OH + CH_3$. More work is needed on the other reaction channel with the $^3A'$ TS, which requires the mapping of PES with the $^3A'$ TS and characterization of the crossing between the two electronic states PESs.

Acknowledgements

The authors thank Professor M. A. Collins for providing the GROW2.2 package and Professor Donald G. Truhlar for providing the POLYRATE 2015 program. The authors thank Professor M. Jordan and Dr. D'Arcy for valuable discussions in the trajectories running on the PES. Many computations are carried out at Virtual Laboratory of Computational Chemistry, Computer Network Information Center of Chinese Academy of Sciences.

References

[1] Zhang J H and Liu K P 2011 *Chem. Asian J.* **6** 3132
[2] Jing F Q, Cao J W, Liu X J, Hu Y F, Ma H T and Bian W S 2016 *Chin. J. Chem. Phys.* **29** 430
[3] Fu B N, Shan X, Zhang D H and Clary D C 2017 *Chem. Soc. Rev.* **46** 7625
[4] Peng Y, Jiang Z A and Chen J S 2017 *J. Phys. Chem. A* **121** 2209
[5] Peng Y, Jiang Z A and Chen J S 2018 *Chin. Phys. B* **27** 023401
[6] Jiang Z A, Peng Y, Chen J S, Lan G and Lin H Y 2018 *Chin. Phys. B* **27** 063401
[7] Ault B S 2019 *J. Mol. Struct.* **1176** 47
[8] Guan Y F and Yarkony D R 2020 *J. Phys. Chem. Lett.* **11** 1848
[9] Liu R, Song H W and Yang M H 2019 *Chinese J Chem. Phys.* **32** 46
[10] Troya D 2019 *J. Phys. Chem. A* **123** 6911
[11] Walch S P and Dunning Jr T H 1980 *J. Chem. Phys.* **72** 3221
[12] Baulch D L, Cobos C, Cox R A *et al.* 1992 *J. Phys. Chem. Ref. Data* **21** 411
[13] Suzuki T and Hirota E 1993 *J. Chem. Phys.* **98** 2387
[14] Wang M L, Li Y M and Zhang J Z 2001 *J. Phys. Chem. A* **105** 2530
[15] Ausfelder F, Kelso H and McKendrick K G 2002 *Phys. Chem. Chem. Phys* **4** 473
[16] Troya D, Schatz G C, Garton D J, Brunsvold A L and Minton T K 2004 *J. Chem. Phys.* **120** 731
[17] Troya D and Garcia-Molina E 2005 *J. Phys. Chem. A* **109** 3015
[18] Zhang J M, Lahankar S A, Garton D J, Minton T K, Zhang W Q and Yang X M 2011 *J. Phys. Chem. A* **115** 10894
[19] Baulch D L, Bowman C T, Cobos C J *et al.* 2005 *J. Phys. Chem. Ref. Data* **34** 757
[20] González C, McDouall J J W and Schlegel H B 1990 *J. Phys. Chem.* **94** 7467
[21] González M, Hernando J, Millán J and Sayós R 1999 *J. Chem. Phys.* **110** 7326
[22] Roberto-Neto O, Machado F B C and Truhlar D G 1999 *J. Chem. Phys.* **111** 10046
[23] Shao K J, Fu B N and Zhang D H 2015 *Chin. J. Chem. Phys.* **28** 403
[24] Corchado J C, Espinosa-Garcia J, Roberto-Neto O, Chuang Y Y and Truhlar D G 1998 *J. Phys. Chem. A* **102** 4899
[25] Czakó G and Bowman J M 2012 *Proc. Natl. Acad. Sci. USA* **109** 7997
[26] Li Y L, Suleimanov Y V, Green W H and Guo H 2014 *J. Phys. Chem. A* **118** 1989
[27] Cederbaum L S, Domcke W and Köppel H 1978 *Chem. Phys.* **33** 319
[28] Domcke W, Mishra S and Poluyanov L V 2006 *Chem. Phys.* **322** 405
[29] Opalka D, Segado M, Poluyanov L V and Domcke W 2010 *Phys. Rev. A* **81** 042501
[30] Czakó G 2014 *J. Chem. Phys.* **140** 231102
[31] Zhao H L, Wang W J and Zhao Y 2016 *J. Phys. Chem. A* **120** 7589
[32] Bowman J M, Czakó G and Fu B N 2011 *Phys. Chem. Chem. Phys.* **13** 8094
[33] González-Lavado E, Corchado J C and Espinosa-Garcia J 2014 *J. Chem. Phys.* **140** 064310
[34] Joseph T, Steckler R and Truhlar D G 1987 *J. Chem. Phys.* **87** 7036
[35] Jordan M J T and Gilbert R G 1995 *J. Chem. Phys.* **102** 5669
[36] Espinosa-Garcia J and Garcia-Bernaldez J C 2000 *Phys. Chem. Chem. Phys.* **2** 2345
[37] Espinosa-Garcia J 2014 *J. Phys. Chem. A* **118** 3572
[38] González-Lavado E, Rangel C and Espinosa-Garcia J 2014 *Phys. Chem. Chem. Phys.* **16** 8428
[39] Monge-Palacios M, González-Lavado E and Espinosa-Garcia J 2014 *J. Chem. Phys.* **141** 094307
[40] Jasper A W, Sivaramakrishnan R and Klippenstein S J 2019 *J. Chem. Phys.* **150** 114112
[41] Suleimanov Y V, Aoiz F J and Guo H 2016 *J. Phys. Chem. A* **120** 8488
[42] Thompson K C, Jordan M J T and Collins M A 1998 *J. Chem. Phys.* **108** 8302
[43] Morris M and Jordan M J T 2014 *J. Chem. Phys.* **140** 204107
[44] Cao J W, Zhang Z J, Zhang C F, Liu K, Wang M H and Bian W S 2009 *Proc. Natl. Acad. Sci. USA* **106** 13180
[45] Zhang W Q, Zhou Y, Wu G R *et al.* 2010 *Proc. Natl. Acad. Sci. USA* **107** 12782
[46] Zhou Y, Fu B N, Wang C R, Collins M A and Zhang D H 2011 *J. Chem. Phys.* **134** 064323
[47] Cao J W, Zhang Z J, Zhang C F, Bian W S and Guo Y 2011 *J. Chem. Phys.* **134** 024315
[48] Frankcombe T J and Collins M A 2011 *Phys. Chem. Chem. Phys.* **13** 8379
[49] Frisch M J, Trucks G W, Schlegel H B *et al.* 2010 *Gaussian 09, Wallingford CT*
[50] Zheng J J, Zhao Y and Truhlar D G 2009 *J. Chem. Theory Comput.* **5** 808
[51] Gomez-Carrasco S, Roncero O, Gonzalez-Sanchez L, Hernandez M L, Alvarino J M, Paniagua M and Aguado A 2005 *J. Chem. Phys.* **123** 114310
[52] Raghavachari K, Trucks G W, Pople J A and Head-Gordon M 1989 *Chem. Phys. Lett.* **157** 479
[53] Bettens R P A and Collins M A 1999 *J. Chem. Phys.* **111** 816
[54] Collins M A 2002 *Theor. Chem. Acc.* **108** 313
[55] Jordan M, Thompson K, Bettens R *et al.* GROW, version 2.2, a collection of scripts and programs that allow the user to construct molecular potential energy surfaces for either unimolecular/bimolecular reactions or bound-state systems
[56] Cao J W, Li F Y, Xia W S and Bian W S 2019 *Chinese J. Chem. Phys.* **32** 157
[57] Wang F Y and Liu K P 2010 *Chem. Sci.* **1** 126
[58] Zheng J, Zhang S, Lynch B J *et al.* POLYRATE, version 2015, a computer program for the calculation of chemical reaction rates for polyatomics, see https://comp.chem.umn.edu/polyrate/
[59] González-Lavado E, Corchado J C, Suleimanov Y V, Green W H and Espinosa-Garcia J 2014 *J. Phys. Chem. A* **118** 3243
[60] Cohen N 1986 *Int. J. Chem. Kinet.* **18** 59
[61] Gordon M S and Truhlar D G 1986 *J. Am. Chem. Soc.* **108** 5412